

Landau theory and giant room-temperature barocaloric effect in MF_3 metal trifluorides

A. Corrales-Salazar¹, R. T. Brierley², P. B. Littlewood^{3,4}, G. G. Guzmán-Verri^{1,4}

¹*Materials Research Science and Engineering Center,
University of Costa Rica, San José, Costa Rica 11501,*

²*Department of Physics, Yale University, New Haven, Connecticut, USA, 06511,*

³*James Franck Institute, University of Chicago, 929 E 57 St, Chicago, Illinois, USA 60637, and*

⁴*Materials Science Division, Argonne National Laboratory, Argonne, Illinois, USA 60439,
(Dated: September 3, 2018)*

The structural phase transitions of MF_3 ($\text{M}=\text{Al}, \text{Cr}, \text{V}, \text{Fe}, \text{Ti}, \text{Sc}$) metal trifluorides are studied within a simple Landau theory consisting of tilts of rigid MF_6 octahedra associated with soft antiferrodistortive optic modes that are coupled to long-wavelength strain generating acoustic phonons. We calculate the temperature and pressure dependence of several quantities such as the spontaneous distortions, volume expansion and shear strains as well as $T - P$ phase diagrams. By contrasting our model to experiments we quantify the deviations from mean-field behavior and found that the tilt fluctuations of the MF_6 octahedra increase with metal cation size. We apply our model to predict giant barocaloric effects in Sc substituted TiF_3 of up to about $15 \text{ JK}^{-1}\text{kg}^{-1}$ for modest hydrostatic compressions of 0.2 GPa. The effect extends over a wide temperature range of over 140 K (including room temperature) due to a large predicted rate $dT_c/dP = 723 \text{ K GPa}^{-1}$, which exceeds those of typical barocaloric materials. Our results suggest that open lattice frameworks such as the trifluorides are an attractive platform to search for giant barocaloric effects.

I. INTRODUCTION

Metal trifluorides (or simply trifluorides) are a class of materials with chemical formula MF_3 ($\text{M}=\text{Al}, \text{Cr}, \text{V}, \text{Fe}, \text{Ti}, \text{Sc}$) and with an open lattice framework in which the trivalent metal ion M is surrounded by an octahedron of corner-shared fluorine atoms.^{1,2} They are isostructural to ReO_3 a well-known ABO_3 perovskite in which the A site is vacant.³ They can exhibit large thermal expansion (TE) which can be reversibly tuned from positive (PTE) to negative (NTE) by temperature, pressure, cation substitution, or redox intercalation.⁴⁻¹⁰ This makes the trifluorides attractive for designing materials that are dimensionally stable and resistant to thermal shocks.¹¹

At ambient pressure, most trifluorides exhibit antiferrodistortive structural transitions with cubic-to-rhombohedral ($c - r$) transformations in which the MF_6 octahedron tilts around the (111) axis. The tilting angles are large, e.g., about 14° in AlF_3 at room temperature (RT)¹² and are accompanied by spontaneous shear and volume strains.¹³ Such lattice instability is the result from the condensation of a three-fold zone-boundary R_4^+ phonon mode of the cubic phase located at the wavevector $(1,1,1)(\pi/a)$.¹⁴ Below the transition, the R_4^+ mode splits into a low energy E_g doublet and a high energy A_{1g} singlet.¹⁵

Density functional theory,¹⁴ molecular dynamics (MD) simulations,¹⁶ and electrostatic energy considerations¹⁷ have shown that the driving force of the lattice instability in the trifluoride is of dipolar origin. When the M-F-M bond bends, fluorine displaces transverse to the bond length generating an electric dipole with a negative end at the F^- anion and a positive end at its cubic lattice site. This distortion concomitantly induces a polarization

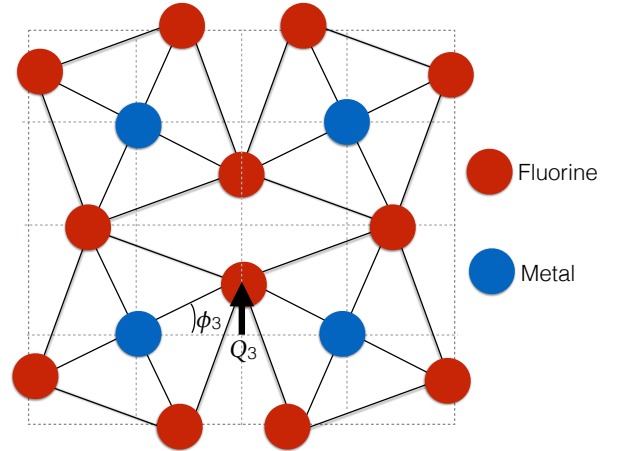


FIG. 1. A (001) section of the MF_3 lattice illustrating the displacement of fluorine ions described by the soft-mode coordinate Q_3 and the antiferrodistortive rotation ϕ_3 of the MF_6 octahedra around (001).

in the fluorine electron cloud that is opposite to the displacive dipole. While there is an energy penalty for creating such induced dipoles, the resulting interactions between the induced-dipoles and between the induced-dipoles with the ionic charges lower the total energy to favor the r -phase over the parent c -structure preferred by the purely ionic Madelung energy.

A trifluoride of special recent interest is ScF_3 , an ionic insulator with a wide indirect energy band gap of about $8 - 10 \text{ eV}$.¹⁸ It does not have a structural transition to an r phase at ambient pressure but rather exhibits incipient behavior in which a nearly flat M-R phonon branch

softens without condensing, as it has been observed by inelastic x-ray scattering experiments (IXS)¹⁹ and found in ab-initio calculations.²⁰ It exhibits strong negative TE (-34 ppm K⁻¹ near RT) from 10 – 1100 K²¹ and and very strong lattice anharmonicities (its soft R_4^+ mode is described by a quartic potential energy in the tilts).²² Its incipient behavior and proximity to a r-phase induced by, e.g., cation substitution^{4,5,7} suggest that ScF₃ is one of the few known stoichiometric materials near a quantum structural phase transition.¹⁹

With hydrostatic compression, the r phase can be induced at higher temperatures. For example, at about 0.6 GPa, a $c - r$ transition is observed near RT in the incipient ScF₃.^{21,23,24} X-ray diffraction experiments have determined the temperature-pressure phase diagrams for Sc substituted AlF₃ (Sc_{1-x}Al_xF₃).⁷ Very significantly, they have observed linearly increasing transition temperatures with pressure with large rates ($dT_c/dP \simeq 400 - 500 \text{ K GPa}^{-1}$) that vary little with Sc concentration and pressure.^{7,21} Additional pressure-induced transitions have been reported at higher pressures.^{23,24}

While microscopic models for the trifluoride are available,^{14,16,17} there is currently no macroscopic approach based on the simple Landau phenomenology. The purpose of this work is thus to construct such a theory. Our model consists of rigid tilts of the MF₆ octahedra associated with the soft R_4^+ optic mode coupled to long-wavelength strain generating acoustic phonons. The model is similar to those used to describe the widely studied antiferrodistortive transitions of SrTiO₃ and LaAlO₃,^{25,26} but with the important distinctions that in the trifluorides the phase transition can be discontinuous and that there are large excess volume strains. By comparing our model to experiments on several trifluorides we quantify the deviations from mean-field behavior and found trends with the metal cation size.

We also apply our model to predict the barocaloric effect (BCE) in the trifluorides. BCEs are reversible thermal changes in a substance in response to changes in hydrostatic pressure and are currently of enormous interest for their potential in developing clean and efficient solid-state cooling technologies.²⁷ It is expected that materials with strong TE such as the trifluorides should give rise to large barocaloric responses, as their entropy rate $(\partial S/\partial P)_T = -(\partial V/\partial T)_P$, according to the Maxwell's relations.²⁷ Indeed, we show that the isothermal changes entropy in the trifluorides are comparable to those of other classes of materials exhibiting so-called giant BCEs,²⁸⁻³⁶ and that it can extend over a broad temperature range which includes RT for modest changes in pressure as a result of their large barocaloric coefficients dT_c/dP . So far, the BCE in the trifluoride has not been studied neither experimentally nor theoretically.

This paper is organized as follows: In Sec. II we present our Landau theory to describe the structural

transitions; in Sec. III we show our results and discussion including a comparison to the isostructural compounds ReO₃ and WO₃; and in Sec. IV we present our conclusions.

II. LANDAU THEORY

A. Free energy

We choose the order parameter as the linear displacement $\mathbf{Q} = (Q_1, Q_2, Q_3)$ which represents, in first order, an antiferrodistortive rotation of the MF₆ octahedra through angles ϕ_i and $-\phi_i$, ($i = 1, 2, 3$) about axes parallel to a cube edge. We normalize the Q 's in such a way that they are numerically equal to the linear fluorine displacements. They are related to ϕ_i by $\tan \phi_i = 2Q_i/a$, where a is the lattice constant, see Fig. 1. In addition to the antiferrodistortive distortion, we introduce elastic strains η_α as a secondary order parameter. We write the components of the strain tensor in the usual Voigt notation: $\eta_\alpha \equiv \epsilon_{\alpha\alpha} = \partial u_\alpha / \partial x_\alpha$ ($\alpha = 1, 2, 3$), $\eta_4 = 2\epsilon_{yz} = 2(\partial u_y / \partial z + \partial u_z / \partial y)$, $\eta_5 = 2\epsilon_{xz} = 2(\partial u_x / \partial z + \partial u_z / \partial x)$, and $\eta_6 = 2\epsilon_{xy} = 2(\partial u_x / \partial y + \partial u_y / \partial x)$. We do not consider fluctuations in \mathbf{Q} and η_α .

Our Landau free energy density is given as follows:

$$G_Q + G_\eta + P \sum_{\alpha=1}^3 \eta_\alpha, \quad (1)$$

where G_Q is a strain-free free energy,

$$\begin{aligned} G_Q = & G_0 + \frac{A}{2} (Q_1^2 + Q_2^2 + Q_3^2) \\ & + \frac{u}{2} (Q_1^2 + Q_2^2 + Q_3^2)^2 + \frac{3v}{2} (Q_1^2 Q_2^2 + Q_1^2 Q_3^2 + Q_2^2 Q_3^2) \\ & + \frac{w_1}{6} (Q_1^2 + Q_2^2 + Q_3^2)^3, \end{aligned} \quad (2)$$

where $A = A_0(T - T_0)$ and T_0 is the supercooling temperature that limits of stability of the parent c-phase. G_η is an energy density with elastic couplings,

$$\begin{aligned} G_\eta = & e_a (\eta_1 + \eta_2 + \eta_3) (Q_1^2 + Q_2^2 + Q_3^2) \\ & - e_t [\eta_1 (2Q_1^2 - Q_2^2 - Q_3^2) + \eta_2 (2Q_2^2 - Q_1^2 - Q_3^2) \\ & \quad + \eta_3 (2Q_3^2 - Q_1^2 - Q_2^2)] \\ & - e_r (Q_1 Q_2 \eta_6 + Q_1 Q_3 \eta_5 + Q_2 Q_3 \eta_4) + \frac{1}{2} \sum_{\alpha\beta} C_{\alpha\beta}^0 \eta_\alpha \eta_\beta. \end{aligned} \quad (3)$$

A_0, u, v, w, e_a, e_t , and e_r are model parameters independent of temperature and pressure and $C_{\alpha\beta}^0$ are the usual elastic constants of the parent phase in the Voigt notation. The third term in the free energy (1) is a hydrostatic compression where P is measured from atmospheric pressure.

In writing the free energy (1), we have not considered any polar degrees of freedom associated with phonon modes that break inversion symmetry as there is no evidence that such lattice modes are unstable in the trifluorides, e.g., the zone-center TO phonon modes do not condense and remain fairly energetic such as in ScF_3 (4 – 5 THz) ^{20,37,38} and other trifluorides. ³⁹ Moreover, Clausius-Mossotti theory predicts that the ground state exhibits antipolar order from the MF_6 tilts with null polarization. ¹⁷ We have also ignored sixth-order cubic anisotropies. Our results will show that this is justified as long as we are describing the r-phase. In Appendix B, we show, however, that they are essential to describe other pressure-induced phases. We have also neglected any polar degrees of freedom associated with phonon modes that would break inversion symmetry, as there is no evidence that such lattice modes are unstable in the trifluorides.

Minimizing Eq. (1) with respect to the strains gives,

$$\begin{aligned}\eta_1 &= -\frac{e_a}{3C_a} (Q_1^2 + Q_2^2 + Q_3^2) \\ &\quad + \frac{e_t}{2C_t} (2Q_1^2 - Q_2^2 - Q_3^2) - \frac{P}{3C_a}, \\ \eta_2 &= -\frac{e_a}{3C_a} (Q_1^2 + Q_2^2 + Q_3^2) \\ &\quad + \frac{e_t}{2C_t} (2Q_2^2 - Q_1^2 - Q_3^2) - \frac{P}{3C_a}, \\ \eta_3 &= -\frac{e_a}{3C_a} (Q_1^2 + Q_2^2 + Q_3^2) \\ &\quad + \frac{e_t}{2C_t} (2Q_3^2 - Q_1^2 - Q_2^2) - \frac{P}{3C_a}, \quad (4) \\ \eta_4 &= \frac{e_r}{C_r} Q_2 Q_3, \\ \eta_5 &= \frac{e_r}{C_r} Q_1 Q_3, \\ \eta_6 &= \frac{e_r}{C_r} Q_1 Q_2,\end{aligned}$$

where $C_a = (1/3)(C_{11}^0 + 2C_{12}^0)$ is the bulk modulus, $C_t = (1/2)(C_{11}^0 - C_{12}^0)$, and $C_r = C_{44}^0$ are the shear tetragonal and rhombohedral moduli, respectively.

When the spontaneous strains of Eq. (4) are substituted back into Eq. (1), we obtain, as expected, ²⁵ that the free energy has the same form as that of Eq. (2) for the strain-free case except with renormalized quadratic (A) and quartic coefficients (u and v) and a

uniform energy shift due to pressure,

$$\begin{aligned}\tilde{G}(T, P) &= G_0 + \frac{1}{2} \tilde{A} (Q_1^2 + Q_2^2 + Q_3^2) \\ &\quad + \frac{\tilde{u}}{2} (Q_1^2 + Q_2^2 + Q_3^2)^2 \\ &\quad + \frac{3\tilde{v}}{2} (Q_1^2 Q_2^2 + Q_1^2 Q_3^2 + Q_2^2 Q_3^2) \quad (5) \\ &\quad + \frac{w_1}{6} (Q_1^2 + Q_2^2 + Q_3^2)^3 \\ &\quad - \frac{1}{2} \frac{P^2}{C_a},\end{aligned}$$

where,

$$\tilde{A} = A - \frac{2e_a P}{C_a}, \quad (6)$$

and,

$$\tilde{u} = u - \left(5 \frac{e_a^2}{C_a} + 3 \frac{e_t^2}{C_t} \right), \quad (7a)$$

$$\tilde{v} = v + \left(3 \frac{e_t^2}{C_t} - \frac{1}{3} \frac{e_r^2}{C_r} \right). \quad (7b)$$

We conclude the presentation of the free energy here. In the next section we apply our model to describe the $c-r$ transition of the trifluorides.

B. $c-r$ transition

The symmetry of the ground state and order of the phase transition is determined by the choice of \tilde{u} and \tilde{v} . For a $c-r$ discontinuous (continuous) transition, we must have $\tilde{v} < 0$ and $\tilde{u} + \tilde{v} < 0$ ($\tilde{u} + \tilde{v} > 0$). ²⁵

To describe the r-phase, we take $\mathbf{Q} = (Q_s/\sqrt{3})(1, 1, 1)$, where Q_s is determined by minimization of the free energy (5),

$$Q_s(T, P) = \pm \left\{ \sqrt{\left(\frac{\tilde{u} + \tilde{v}}{w_1} \right)^2 - \frac{\tilde{A}}{w_1}} - \left(\frac{\tilde{u} + \tilde{v}}{w_1} \right) \right\}^{1/2}. \quad (8)$$

Substitution of the order parameter (8) into Eq. (4) gives, respectively, the following the spontaneous volume and shear strains,

$$\eta_a = \eta_1 + \eta_2 + \eta_3 = -\frac{e_a}{C_a} Q_s^2 - P/C_a, \quad (9a)$$

$$\eta_r = \eta_4 = \eta_5 = \eta_6 = \frac{e_r}{3C_r} Q_s^2 = \cos \alpha_C, \quad (9b)$$

where α_C as the angle between any two axes of the c unit cell.

Experiments ^{5,7,12} usually report the ratio between the lattice constants c_H and a_H of a hexagonal unit cell,

$$\frac{c_H}{a_H} = \sqrt{\frac{3}{2} \frac{1 + 2 \cos \alpha_R}{1 - \cos \alpha_R}}. \quad (10)$$

where α_R is the angle between any two vectors of a r-unit cell. α_R and α_C are related as follows:

$$\cos \alpha_R = \frac{1}{2} \frac{1 + 3 \cos \alpha_C}{1 + \cos \alpha_C}. \quad (11)$$

We now derive expressions for the relevant temperature scales. From Q_s of Eq. (8), we find that the stability of the r phase ends at the superheating temperature,

$$T^*(P) = T^*(0) + \left(\frac{2}{A_0} \frac{e_a}{C_a} \right) P, \quad (12)$$

where $T^*(0) = T_0 + \frac{w_1}{A_0} \left(\frac{\bar{u} + \bar{v}}{w_1} \right)^2$ is the superheating temperature at ambient pressure. By equating the free energies \tilde{G}_Q of the high and low temperature phases, we find the transition temperature,

$$T_c(P) = T_c(0) + \left(\frac{2}{A_0} \frac{e_a}{C_a} \right) P, \quad (13)$$

where $T_c(0) = T_0 + \frac{3}{4} \frac{w_1}{A_0} \left(\frac{\bar{u} + \bar{v}}{w_1} \right)^2$ is the transition temperature at ambient pressure. In the next sections, we calculate several thermodynamic quantities of interest.

1. Coefficient of thermal expansion, entropy, latent heat, heat capacity, and barocaloric effect

We begin with the volume change with temperature and the coefficient of thermal expansion (CTE). The temperature and pressure dependence of the volume V is given by,⁴⁰

$$V(T)/V_0 = \frac{\partial \tilde{G}}{\partial P} = \begin{cases} 1 - \frac{P}{C_a}, & T > T_c \\ 1 - \frac{e_a}{C_a} Q_s^2 - \frac{P}{C_a}, & T < T_c. \end{cases} \quad (14)$$

V_0 is a reference volume and $(\partial G_0/\partial P) = 1$. As expected, the relative change in volume in the r -phase is equal to the volumetric strain $\eta_1 + \eta_2 + \eta_3$. The CTE is given as follows:

$$\begin{aligned} \kappa(T) &= \frac{\partial^2 \tilde{G}}{\partial T \partial P}, \\ &= \begin{cases} (\partial V_0/\partial T) = \kappa_0, & T > T_c \\ \kappa_0 + \frac{1}{2} \frac{e_a}{C_a} \frac{A_0/w_1}{\sqrt{\left(\frac{\bar{u} + \bar{v}}{w_1}\right)^2 - \frac{A}{w_1}}}, & T < T_c. \end{cases} \end{aligned} \quad (15)$$

We calculate the entropy per unit volume from the free energy of Eq. (5),

$$S(T, P) = -\frac{\partial \tilde{G}}{\partial T} = \begin{cases} S_0, & T > T_c, \\ S_0 - \frac{A_0}{2} Q_s^2, & T < T_c. \end{cases} \quad (16)$$

The latent heat per unit volume of the transition at $P = 0$ is then given as follows,

$$T_c \Delta S(T_c, 0) = T_c \times \frac{A_0}{2} Q_s^2(T_c, 0), \quad (17)$$

where $\Delta S(T_c, 0)$ is the entropy jump at the $c - r$ transition.

We now calculate the heat capacity per unit volume,

$$\begin{aligned} C_P &= T \frac{\partial S(T, P)}{\partial T} \\ &= \begin{cases} C_P^0, & T > T_c, \\ C_P^0 + T \frac{A_0}{4} \frac{A_0/w_1}{\sqrt{\left(\frac{\bar{u} + \bar{v}}{w_1}\right)^2 - \frac{A}{w_1}}}, & T < T_c, \end{cases} \end{aligned} \quad (18)$$

where $C_P^0 = T (\partial S_0/\partial T)$ is a reference heat capacity in the high temperature phase.

From Eq. (16), we calculate the isotropic changes in entropy,

$$\Delta S(T, P) = \begin{cases} 0, & T > T_c, \\ -\frac{A_0}{2} (Q_s^2(T, P) - Q_s^2(T, 0)), & T < T_c. \end{cases} \quad (19)$$

We conclude the presentation of our model here. In the next section we apply it to several trifluorides.

III. RESULTS AND DISCUSSION

A. Fits and comparison to experiments

We now discuss our fits to several trifluoride compounds. For pure TiF_3 and AlF_3 , we fit our model to their observed c_H/a_H , M-F-M bond angle, volume expansion, CTE and latent heat of the transition,^{2,5,7,12} see Fig. 2. For $\text{Sc}_{1-x}\text{Al}_x\text{F}_3$ with $x < 1$, we do a slightly different fit since their latent heats are unknown: we fix the ratio $dT_c/dP = 2e_a/(A_0C_a)$ to that of the pure compound AlF_3 . This is justified by the observed linear $T - P$ phase diagram of $\text{Sc}_{1-x}\text{Al}_x\text{F}_3$ with a slope that varies little with composition x .⁷ We do a similar fit for $\text{Sc}_{1-x}\text{Ti}_x\text{F}_3$. The resulting parameters together with the calculated supercooling and superheating temperatures are given in Table I.

Overall, we find that there is good agreement between our model and experiments. The discrepancies between the observed and calculated M-F-M bond angles above T_c shown in Figs. 2 (g) and (h), are due to local lattice distortions from the average c -structure,^{16,41} which we have not considered in our model. More importantly, the deviations from mean-field behavior are most noticeable in the volume expansions of ScF_3 and AlF_3 , (see Figs. 2 (c) and (d)), which correspond to the extreme cases of large and small metal ion radius considered in this work ($r_{\text{Sc}} = 0.745 \text{ \AA}$, $r_{\text{Al}} = 0.535 \text{ \AA}$). This suggests a trend with M-cation size. In ScF_3 , NTE is the result of cooperative tilt fluctuations of the rigid ScF_6 octahedra which reduce the average Sc-Sc distance while keeping the Sc-F distance fixed. Such fluctuations can only give rise to NTE; therefore the PTE in AlF_3 must originate from non rigid modes such as Al-F bond stretching, which we have not considered in our model.

$\text{Sc}_{1-x}\text{Ti}_x\text{F}_3$ with $x = 0.7$ has a mean B site radius in between these two extremes (0.69 Å) and the deviations from our model and its observed volume expansion are tiny, which indicates that the fluctuations of both rigid and non-rigid modes are unimportant. A picture

TABLE I. Model parameters for $\text{Sc}_{1-x}\text{Al}_x\text{F}_3$ and $\text{Sc}_{1-x}\text{Ti}_x\text{F}_3$ and predicted supercooling (T_0) and superheating (T^*) temperatures at ambient pressure. Transition temperatures (T_c) taken from Refs. [5, 7, and 12]

	$\text{Sc}_{1-x}\text{Al}_x\text{F}_3$		$\text{Sc}_{1-x}\text{Ti}_x\text{F}_3$	
	$x = 1.0$	$x = 0.4$	$x = 1.0$	$x = 0.7$
$\kappa_0 [10^{-6} \text{ K}^{-1}]$	10	10	0	0
$\tilde{u} + \tilde{v} [\text{meV } \text{\AA}^{-7}]$	-0.78	0.05	-0.81	-0.27
$A_0 [10^{-3} \text{ meV K}^{-1} \text{\AA}^{-5}]$	3.7	5.8	2.9	3.1
$w [\text{meV } \text{\AA}^{-9}]$	12	48	13	17
$e_a/C_a [\text{\AA}^{-2}]$	0.13	0.20	0.17	0.17
$e_r/C_r [\text{\AA}^{-2}]$	0.14	0.27	0.28	0.30
$T_0 [\text{K}]$	703	493	327	227
$T^* [\text{K}]$	718	493	344	228
$T_c [\text{K}]$	713	493	340	228

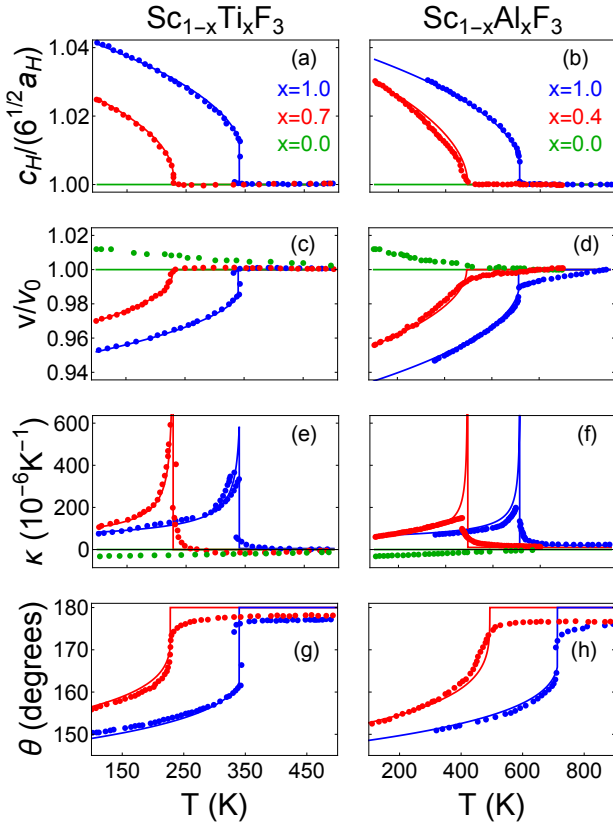


FIG. 2. Comparison between our model (solid line) and experiments (dots) for the temperature dependence of (a,b) ratio hexagonal lattice constants, (c,d) unit cell volume, (e,f) CTE, and (g,h) metal-F-metal bond angle θ in $\text{Sc}_{1-x}\text{Ti}_x\text{F}_3$ and $\text{Sc}_{1-x}\text{Al}_x\text{F}_3$. Data taken from Refs. [5, 7, and 12].

therefore emerges in which rigid octahedra fluctuations

dominate the TE for large metal ions and decrease with their size, while non rigid vibrational modes dominate the TE for small metal ions and decrease with increasing radius.

Fig. 3 shows the predicted spontaneous shear strains, order parameter, and specific heats for $\text{Sc}_{1-x}\text{Al}_x\text{F}_3$ and $\text{Sc}_{1-x}\text{Ti}_x\text{F}_3$ using our parametrization. Our prediction for the shear strains in AlF_3 compares well with experiments.¹³

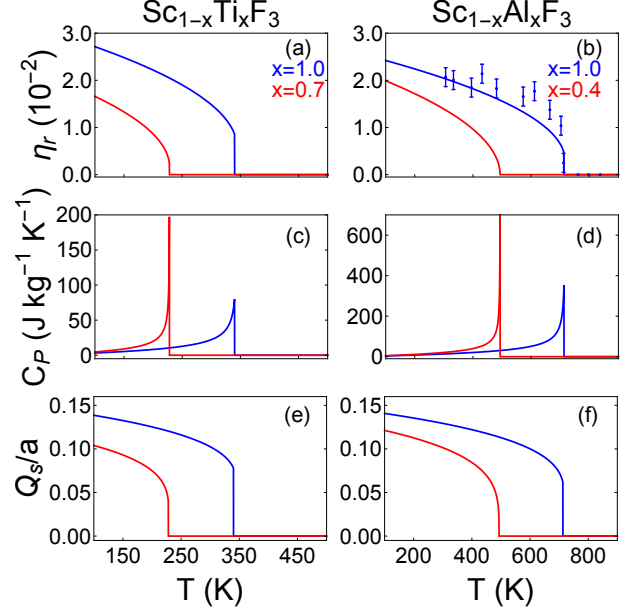


FIG. 3. (a,b) Spontaneous shear strains, (c,d) excess specific heat, and (e,f) order parameter predicted from the fits obtained from Fig. 2 for $\text{Sc}_{1-x}\text{Ti}_x\text{F}_3$ and $\text{Sc}_{1-x}\text{Al}_x\text{F}_3$. Measured spontaneous strains (dots) taken from Ref. [13].

Figures 4 (a) and (b) show the $T - P$ phase diagrams of $\text{Sc}_{1-x}\text{Ti}_x\text{F}_3$ and $\text{Sc}_{1-x}\text{Al}_x\text{F}_3$ calculated from Eq. (13). The linear dependence between T and P of our model agrees with the observed phase diagram for $\text{Sc}_{1-x}\text{Al}_x\text{F}_3$.^{7,21} Using Eq. (13) and the parameters from Table I, we find that $dT_c/dP \simeq 0.4 \times 10^3 \text{ K GPa}^{-1}$ which is in excellent agreement with experiments.^{7,21} For $\text{Sc}_{1-x}\text{Ti}_x\text{F}_3$, we predict that $dT_c/dP \simeq 0.7 \times 10^3 \text{ K GPa}^{-1}$. There are no reports on the calculated or measured $T - P$ phase diagram for $\text{Sc}_{1-x}\text{Ti}_x\text{F}_3$ in the literature.

In Appendix A, we derive expressions for the temperature dependence of the soft mode frequencies. In the parent c phase, we find the usual mean field behavior for the R_4^+ mode, $\omega_{R_4^+} \propto \sqrt{A_0(T - T_0)}$, which is in agreement with IXS.¹⁹ In addition, our values for A_0 given in Table I are about what is expected from the observed soft mode ($A_0 \simeq 3 \times 10^{-3} \text{ meV K}^{-1} \text{\AA}^{-5}$) for ScF_3 .¹⁹ The temperature dependence of the A_{1g} and E_g phonon frequencies in the r phase has been measured by Raman scattering experiments for AlF_3 ,² however, we cannot compare to our model as the shear moduli C_t and

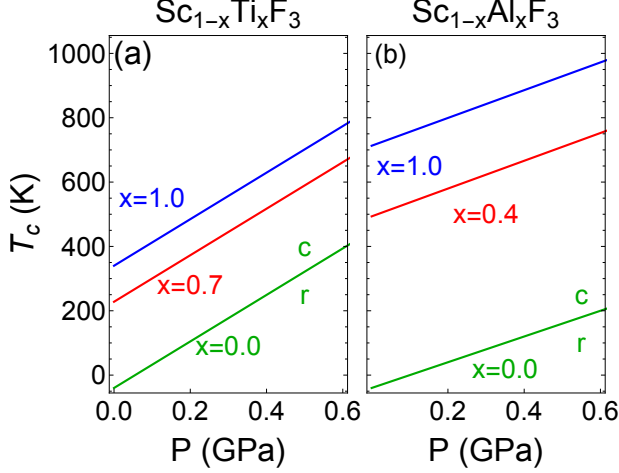


FIG. 4. Calculated $T - P$ phase diagrams for (a) $\text{Sc}_{1-x}\text{Ti}_x\text{F}_3$ and (b) $\text{Sc}_{1-x}\text{Al}_x\text{F}_3$.

C_r are unknown.

B. Barocaloric effect

Figure 5 shows the predicted BCE for $\text{Sc}_{1-x}\text{Ti}_x\text{F}_3$ ($x = 0.85$) calculated from Eq. (19). We have chosen this composition as its $c - r$ transition occurs near RT ($T_c = 283\text{ K}$) and exhibits a strong first order character.⁵ As expected from the large CTEs, the resulting isothermal changes in entropy are comparable to those exhibiting giant effects,³⁴ as it is shown in Table II. Moreover, the effect extends over a temperature range of about 140 K for pressure changes of 0.2 GPa which includes RT. The wide temperature range is a consequence of the large predicted value of $dT_c/dP (= 723\text{ K GPa}^{-1})$, which exceeds those of typical barocaloric compounds, see Table II. The inset in Fig. 5 shows the expected monotonic growth of maximum entropy changes at T_c , ΔS_{max} , with changes in pressure.

C. Comparison to ReO_3

It is interesting to compare ScF_3 with the isostructural compound ReO_3 . At ambient pressure, ReO_3 exhibits a perovskite c lattice structure from the lowest observed temperature up to its melting point despite its empty A site and therefore low tolerance factor.³ The stability of the c phase is a consequence of its metallicity: the Fermi pressure of delocalized Re $5d$ electrons that occupy the π^* conduction band keep the ReO_6 octahedra from tilting.⁴² On the other hand, such states are empty in the wide-gap insulator ScF_3 .¹⁸ Its lattice

structure remains cubic at all temperatures due to its purely ionic Madelung energy.¹⁴ Both compounds exhibit

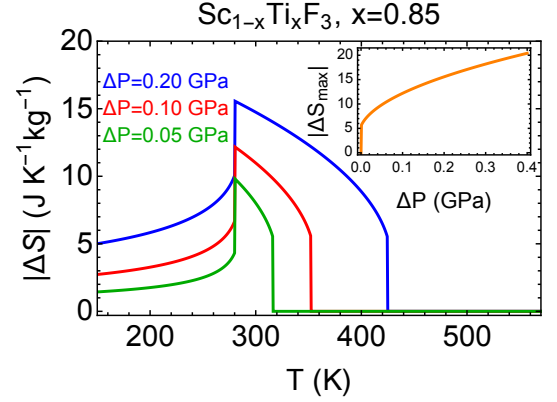


FIG. 5. Calculated isothermal changes in entropy for $\text{Sc}_{1-x}\text{Ti}_x\text{F}_3$, $x = 0.85$. Inset: Pressure dependence of the maximum changes in entropy.

incipient lattice instabilities in their c -phases. In ScF_3 , softening of the entire M-R phonon branch (with lowest point at R) has been observed by IXS¹⁹ from 300 to 8 K at ambient pressure and also found by a first-principles calculation.²⁰ The temperature dependence of the phonon energies is well-described by mean-field theory, as discussed above. Condensation of the R_4^+ mode and its associated $c - r$ transition can be induced by modest hydrostatic compression ($\sim 0.6\text{ GPa}$ at RT)^{21,23,24} or cation substitution.^{4,5,7} It is unknown whether the transition is of first or second order. In ReO_3 , inelastic neutron scattering experiments⁴³ (INS) have observed softening from 280 to 2 K without condensation of the M_3^+ phonon mode, which consists of in-phase rotations of rigid ReO_6 octahedra along a $[100]$ axis that passes through the metal cation. The supposedly observed linear temperature dependence of the mode energy is unusual as it is shown by the blue dashed line in Fig. 6. However, we make the observation that the linear fit is hardly distinguishable from the standard mean-field behavior, $\omega_{\text{M}_3^+} \propto \sqrt{A_0(T - T_0)}$, with physically reasonable parameters ($A_0 \simeq 2.5 \times 10^{-3}\text{ meV K}^{-1} \text{ \AA}^{-5}$, and $T_0 \simeq -296\text{ K}$), see solid red line in Fig. 6. The mode can be condensed upon application of moderate pressures ($\sim 0.5\text{ GPa}$ at RT) and a $P - T$ phase diagram has been established by neutron diffraction experiments⁴⁴ in which the high-pressure phase has c symmetry ($Im\bar{3}$) and the transition line is of second-order.⁴⁵ Additional pressure-induced transitions have been reported in ScF_3 ^{23,24} and ReO_3 ⁴⁶ at higher pressures.

Both ScF_3 ²¹ and ReO_3 ⁴⁷⁻⁴⁹ exhibit negative TE over a wide temperature range with a common origin: large quartic anharmonicities of their corresponding soft R_4^+ and M_3^+ modes consisting of rigid antiphase rotations of the ScF_6 and ReO_6 octahedra, respectively.^{22,43} The size of the effect, however, is an order of magnitude larger in

TABLE II. Transition temperatures (T_c), isothermal entropy changes (ΔS), isothermal heats ($Q = T_c \Delta S$), pressure changes (ΔP), caloric strengths ($\Delta S/\Delta P$), refrigerant capacity (RC), and $T - P$ slope (dT_c/dP) of giant barocaloric materials.

Compound	T_c [K]	ΔS [JK ⁻¹ kg ⁻¹]	Q [kJkg ⁻¹]	ΔP [GPa]	$\frac{\Delta S}{\Delta P}$ [JK ⁻¹ kg ⁻¹ GPa ⁻¹]	RC [Jkg ⁻¹]	$\frac{dT_c}{dP}$ [KGPa ⁻¹]	Ref.
Ni _{49.26} Mn _{36.08} In _{14.66}	293	24	7.0	0.26	92	120	18	28
LaFe _{11.33} Co _{0.47} Si _{1.2}	237	8.7	2.0	0.20	43.5	81	73	29
(NH ₄) ₃ MoO ₃ F ₃	297	55	16.3	0.5	110	5200	202	30
Gd ₅ Si ₂ Ge ₂	270	11	2.9	0.20	55	180	32	31
Fe ₄₉ Rh ₅₁	308	12.5	3.8	0.11	114	105	54	32
Mn ₃ GaN	285	21.6	6.2	0.09	240	125	65	33
(NH ₄) ₂ SO ₄	219	60	13.2	0.10	600	276	45	34
BaTiO ₃	400	1.6	0.64	0.10	16	10	-58	35
[TPrA] [Mn(dca) ₃]	330	35.1	11.6	0.00689	5094	62	231	36
Sc _{1-x} Ti _x F ₃ ($x = 0.85$)	283	12	3.4	0.10	120	406	723	This work

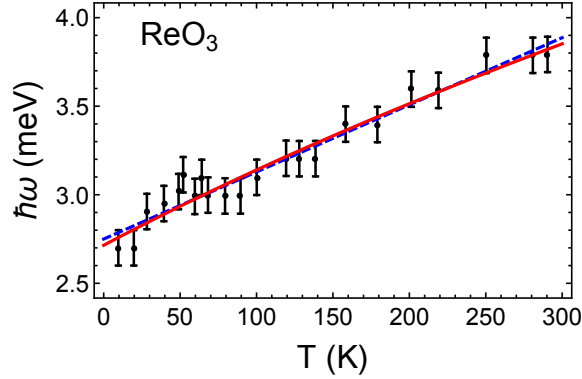


FIG. 6. Temperature dependence of the M_3^+ phonon mode in ReO_3 . Dashed-blue and solid-red lines correspond to purely linear and classical mean-field behavior, respectively. Data taken from Ref. [43]

ScF_3 than in ReO_3 . This can be understood from the distinct nature of their metal-nonmetal bonds. In ScF_3 , there is little overlap between the charge densities that form the ionic bond between Sc^{3+} and F^- ,³⁸ which favors large buckling fluctuations in the Sc-F-Sc chains. In ReO_3 , the buckling fluctuations of the Re-O-Re bonds are reduced by the stiffer covalent bond formed by hybridized Re 5d and O 2p electrons.^{42,50}

D. Comparison to WO_3

Another interesting compound to compare with is tungsten bronze WO_3 . Like ScF_3 , WO_3 is an insulator but its high temperature phase is tetragonal (t) and it goes through several structural transitions upon cooling.³ Its hypothetical c structure has an unstable M_3^- mode consisting of opposite displacements of the cations and anions from unit cell to unit cell along the [110] directions,⁵¹ which generate off-center displacements of W^{6+} towards one of its nearest O^{2-} with concomitant increase in their covalency.⁵² Condensation of this mode leads to a t -structure of highly distorted WO_6 octahedra.⁵³ The energy gain due to the increase in

covalency between W^{6+} and O^{2-} favors the t phase over the ionic c -structure.⁵² The c phase can be stabilized in WO_3 by introducing electrons: when doped with Na, 3s electrons begin to occupy the conduction band and, for sufficiently large concentrations, their Fermi pressure stabilizes the c phase.⁵⁰ Such a c phase displays PTE and mean-field softening with temperature of its M_3^- phonon mode down to about 416 K where a structural transition to a t phase occurs.⁵⁴

IV. CONCLUSIONS

We have presented a Landau theory for trifluoride and have used it to calculate and predict the temperature and pressure dependence of several thermodynamic quantities. We have compared our results to existing experimental data on trifluorides and have quantified the deviations from mean-field theory. We have found that the fluctuations of their rigid MF_6 octahedra tend to increase with the metal cation size. We have used our model to predict a giant BCE in $\text{Sc}_{1-x}\text{Ti}_x\text{F}_3$ ($x = 0.85$) of up to 15 JK⁻¹kg⁻¹ for a pressure change of 0.2 GPa. This effect extends over a temperature range of over 140 K, which includes RT. Our results suggest that open lattice frameworks such as the trifluorides could be a promising platform to search for giant barocaloric effects.

V. ACKNOWLEDGMENTS

GGGV thanks Xavier Moya and Esteban Avedaño for useful discussions and Jason Hancock and Sahan Handunkanda for carefully reading the manuscript. Work at the University of Costa Rica is supported by the Vice-rectory for Research under the project no. 816-B5-220, and work at Argonne National Laboratory is supported by the U.S. Department of Energy, Office of Basic Energy Sciences, Material Sciences and Engineering Division under contract no. DE-AC02-06CH11357. GGGV and RTB acknowledge partial financial support from the Office of International Affairs at the University of Costa Rica.

Appendix A: Soft Mode Frequencies

The soft mode frequencies are computed from the free energy (2) with the η 's constant,²⁶

$$\varrho(\omega_i)^2 \delta_{ij} = \frac{\partial^2(G_Q + G_\eta)}{\partial \hat{Q}_i \partial \hat{Q}_j}, \quad (i, j = 1, 2, 3) \quad (\text{A1})$$

where \hat{Q}_i are principal-axis coordinates of the soft mode and $\varrho = 2m_F/a^3$ is the mass density of fluorine atoms participating in each mode, where m_F is the mass of the fluorine atom. The soft mode frequencies given in Eq. (A1) must be evaluated at the equilibrium points given in Eqs. (8) and (4). The free energy G appearing in Eq. (A1) is that of Eq. (2) rather than that of Eq. (5) because the frequency of the acoustic modes associated with uniform strains vanishes in the long-wavelength limit.²⁶

In the c phase, the frequency of the R_4^+ mode is threefold degenerate since all strains vanish,

$$\varrho \omega_{R_4^+}^2 = \tilde{A}. \quad (\text{A2})$$

In the r phase, the mode splits into the E_g doublet and the A_{1g} singlet,

$$\varrho \omega_{E_g}^2 = \tilde{A} + \left(2\tilde{u} + 8\frac{e_a^2}{C_a} + 6\frac{e_t^2}{C_t} + \frac{1}{3}\frac{e_r^2}{C_r} + w_1 Q_s^2 \right) Q_s^2, \quad (\text{A3a})$$

$$\varrho \omega_{A_{1g}}^2 = \tilde{A} + \left(6[\tilde{u} + \tilde{v}] + 28\frac{e_a^2}{C_a} + \frac{4}{3}\frac{e_r^2}{C_r} + 5w_1 Q_s^2 \right) Q_s^2, \quad (\text{A3b})$$

where Q_s is given in Eq. (8).

Appendix B: Sixth-order c anisotropy

In this Appendix, we discuss the effects of sixth-order anisotropies in some of our previous results. We will show that such anisotropies allow us to describe a possible phase competition between pressure-induced phases. So far, the evidence for phase competition has been experimentally reported in ScF_3 ^{23,24} where near about 3.0 GPa, the r phase destabilizes and a structural transition to an orthorhombic (o) phase occurs. In addition, a MD simulation of AlF_3 has found a metastable o -phase in the free energy at ambient pressure and below the $c - r$ transition temperature.¹⁶ No $r - o$ transition has been observed in TiF_3 , FeF_3 , and CrF_3 .^{55,56}

It is well known that the free energy (5) does not support a stable o phase.²⁵ To include it, we must add sixth-order c anisotropies,

$$\begin{aligned} & \frac{3w_2}{4} (Q_1^2(Q_2^4 + Q_3^4) + Q_2^2(Q_1^4 + Q_3^4) \\ & + Q_3^2(Q_1^4 + Q_2^4)) \\ & + \frac{9w_3}{2} Q_1^2 Q_2^2 Q_3^2. \end{aligned} \quad (\text{B1})$$

where w_2 and w_3 are parameters independent of temperature and pressure. We consider the following order parameters for the t -, o - and r -phases,

$$t : (Q_1, Q_2, Q_3) = Q_s (0, 0, 1),$$

$$o : (Q_1, Q_2, Q_3) = \frac{Q_s}{\sqrt{2}} (1, 1, 0),$$

$$r : (Q_1, Q_2, Q_3) = \frac{Q_s}{\sqrt{3}} (1, 1, 1).$$

The contribution from the anisotropic terms of Eq. (B1) to the free energy is,

$$\tilde{G}_{AN}(t) = 0, \quad (\text{B2a})$$

$$\tilde{G}_{AN}(o) = \left(\frac{3}{8}\tilde{v} + \frac{3}{16}w_2 Q_s^2 \right) Q_s^4, \quad (\text{B2b})$$

$$\tilde{G}_{AN}(r) = \left(\frac{1}{2}\tilde{v} + \frac{1}{6}(w_2 + w_3) Q_s^2 \right) Q_s^4. \quad (\text{B2c})$$

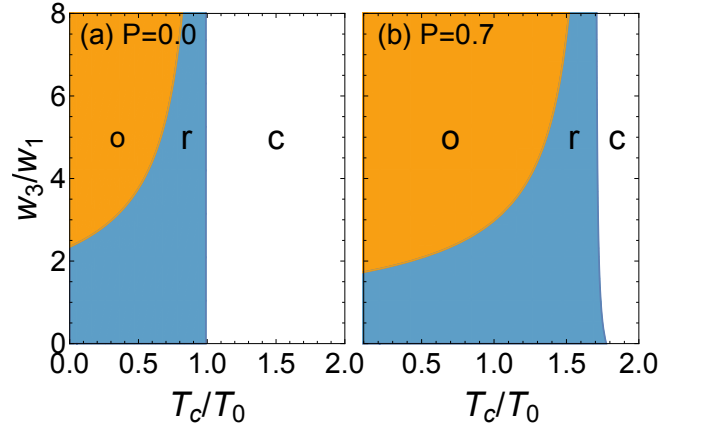


FIG. 7. Schematic phase diagrams of the trifluoride (a) at ambient pressure and (b) with applied hydrostatic compression. All transition lines are of first-order. Here, $A_0 T_0 / (w_1 a^4) = 1.0 \times 10^{-3}$, $\tilde{u} / (w_1 a^2) = 6.0 \times 10^{-2}$, and $\tilde{v} / (w_1 a^2) = -7.0 \times 10^{-2}$. P is in units of $C_a A_0 T_0 / (2e_a)$.

For simplicity, we take $w_2 = 0$. Then, for $\tilde{v} < 0$ and $w_1 + w_3 > 0$, we find that the r phase is the global minimum for small spontaneous distortions ($Q_s^2 < -(3/4)(\tilde{v}/w_3)$) while the o phase is a local minimum; and viceversa for large distortions [$Q_s^2 > -(3/4)(\tilde{v}/w_3)$]. For $\tilde{v} < 0$ and $w_1 + w_3 \leq 0$, the energy has unphysical divergences implying that higher-order terms must be taken into account. The t phase is always metastable.

The order parameter of the o phase with $w_2 = 0$ is given as follows,

$$Q_s(T, P) = \pm \left\{ \sqrt{\left(\frac{\tilde{u} + 3\tilde{v}/4}{w_1} \right)^2 - \frac{\tilde{A}}{w_1}} - \left(\frac{\tilde{u} + 3\tilde{v}/4}{w_1} \right) \right\}^{1/2},$$

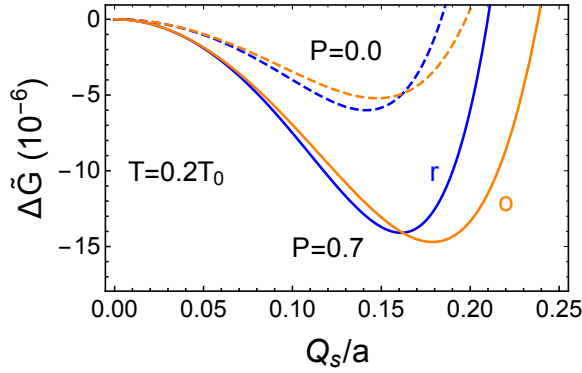


FIG. 8. Free energy densities for $w_3/w_1 = 2.0$. $\Delta\tilde{G}$ and P are in units of $w_1 a^6$ and $C_a A_0 T_0 / (2e_a)$, respectively.

where \tilde{A} is given by Eq. (6). The order parameter of the r-phase with sixth-order anisotropies is obtained by replacing $w_1 \rightarrow w_1 + w_3$ in Eq. (8).

Figure 7(a) shows a generic $w_3 - T$ phase diagram

at ambient pressure calculated by comparing the free energies of the c , r and o minima. For small anisotropies ($w_3/w_1 \lesssim 2.2$), we find there is only a $c - r$ phase transition; while for large anisotropies ($w_3/w_1 \gtrsim 2.2$), an additional $r - o$ phase change occurs at low temperatures. Figure 7(b) shows the $w_3 - T$ phase diagram at an applied pressure. As expected, pressure favors ordering: as the $c - r$ and $r - o$ transitions are pushed to higher temperatures. The corresponding free energy changes $\Delta\tilde{G} = \tilde{G} - G_0 + P^2/(2C_a)$ of the r and o phases for $w_3/w_1 = 2.0$ are shown in Fig. 8. The free energy of the metastable t phase is not shown for clarity. At ambient pressure, the r phase is a global minimum while the o phase is metastable, which is in agreement with MD simulations.¹⁶ With large enough applied pressures, the situation reverses and the r-phase becomes a local minimum while the o phase is the ground state. Metal trifluorides must then lie in the region of low anisotropy ($w_3/w_1 < 2.2$), as no transition to an o phase has been observed at ambient pressure.

- ¹ M. A. Hepworth, K. H. Jack, R. D. Peacock, and G. J. Westland, "The crystal structures of the trifluorides of iron, cobalt, ruthenium, rhodium, palladium and iridium," *Acta Crystallogr.* **10**, 63 (1957).
- ² P. Daniel, A. Bulou, M. Rousseau, J. Nouet, and M. Leblanc, "Raman-scattering study of crystallized MF₃ compounds (M=Al, Cr, Ga, V, Fe, In): an approach to the short-range-order force constants," *Phys. Rev. B* **42**, 10545 (1990).
- ³ N. Tsuda, K. Nasu, A. Fujimori, and K. Siratori, *Electronic Conduction in Oxides* (Springer, 2000).
- ⁴ C. R. Morelock, B. K. Greve, L. C. Gallington, K. W. C., and A. P. Wilkinson, "Negative thermal expansion and compressibility of Sc_{1-x}Y_xF₃ ($x \leq 0.25$)," *J. Appl. Phys.* **114**, 213501 (2013).
- ⁵ C. R. Morelock, L. C. Gallington, and A. P. Wilkinson, "Evolution of negative thermal expansion and phase transitions in Sc_{1-x}Ti_xF₃," *Chem. Mater.* **26**, 1936 (2014).
- ⁶ L. Hu, J. Chen, L. Fan, Y. Ren, Y. Rong, Z. Pan, J. Deng, R. Yu, and X. Xing, "Zero thermal expansion and ferromagnetism in cubic Sc_{1-x}M_xF₃ (M = Ga, Fe) over a wide temperature range," *J. Am. Chem. Soc.* **136**, 13566 (2014).
- ⁷ C. R. Morelock, L. C. Gallington, and A. P. Wilkinson, "Solid solubility, phase transitions, thermal expansion, and compressibility in Sc_{1-x}Al_xF₃," *J. Solid State Chem.* **222**, 96 (2015).
- ⁸ C. P. Romao, C. R. Morelock, A. P. Wilkinson, and M. Anne, "The heat capacities of thermomiotic ScF₃ and ScF₃-YF₃ solid solutions," *J. Mater. Sci.* **50**, 3409 (2015).
- ⁹ T. Wang, J. Xu, L. Hu, W. Wang, R. Huang, F. Han, Z. Pan, J. Deng, Y. Ren, L. Li, J. Chen, and X. Xing, "Tunable thermal expansion and magnetism in Zr-doped ScF₃," *Appl. Phys. Lett.* **109**, 181901 (2016).
- ¹⁰ J. Chen, Q. Gao, A. Sanson, X. Jiang, Q. Huang, A. Carnera, C. G. Rodriguez, L. Olivi, L. Wang, L. Hu, K. Lin, Y. Ren, Z. Lin, C. Wang, L. Gu, J. Deng, J. P. Attfield, and X. Xing, "Tunable thermal expansion in framework materials through redox intercalation," *Nat. Commun.* **8**, 14441 (2017).
- ¹¹ L. Wang, C. Wang, Y. Sun, K. Shi, S. Deng, H. Lu, P. Hu, and X. Zhang, "Metal fluorides, a new family of negative thermal expansion materials," *J. Materiomics* **1**, 106 (2015); J. Chen, L. Hu, J. Deng, and X. Xing, "Negative thermal expansion in functional materials: controllable thermal expansion by chemical modifications," *Chem. Soc. Rev.* **44**, 3522-3567 (2015); C. P. Romao, K. J. Miller, C. A. Whitman, M. A. White, and B. A. Marinkovic, "4.07 - negative thermal expansion (thermomiotic) materials," in *Comprehensive Inorganic Chemistry II (Second Edition)*, edited by J. Reedijk and K. Poeppelmeier (Elsevier, Amsterdam, 2013) second edition ed., p. 127; C. Lind, "Two decades of negative thermal expansion research: where do we stand?" *Materials* **5**, 1125 (2012); W. Miller, C. W. Smith, D. S. Mackenzie, and K. E. Evans, "Negative thermal expansion: a review," *J. Mat. Sci.* **44**, 5441-5451 (2009).
- ¹² C. R. Morelock, J. C. Hancock, and A. P. Wilkinson, "Thermal expansion and phase transitions of α -AlF₃," *J. Solid State Chem.* **219**, 143 (2014).
- ¹³ B. J. Kennedy and T. Vogt, "Powder X-ray diffraction study of the rhombohedral to cubic phase transition in TiF₃," *Mat. Res. Bull.* **37**, 77 (2002).
- ¹⁴ Y.-R. Chen, V. Perebeinos, and P. B. Allen, "Density-functional study of the cubic-to-rhombohedral transition in α -AlF₃," *Phys. Rev. B* **69**, 054109 (2004).
- ¹⁵ P. Daniel, A. Bulou, M. Rousseau, J. Nouet, J. L. Fourquet, M. Leblanc, and R. Burriel, "A study of the structural phase transitions in AlF₃: x-ray powder diffraction, differential scanning calorimetry (DSC) and Raman scattering investigations of the lattice dynamics and phonon spectrum," *J. Phys. Condens. Matter* **2**, 5663 (1990).

- ¹⁶ S. Chaudhuri, P. J. Chupas, M. Wilson, P. Madden, and C. P. Grey, "Study of the nature and mechanism of the rhombohedral-to-cubic phase transition in α -AlF₃ with molecular dynamics simulations," *J. Phys. Chem. B* **108**, 3437 (2004).
- ¹⁷ P. Allen, Y.-R. Chen, S. Chaudhuri, and C. Grey, "Octahedral tilt instability of ReO₃-type crystals," *Phys. Rev. B* **73**, 172102 (2006).
- ¹⁸ D. Bocharov, P. Žgurs, S. Piskunov, A. Kuzmin, and J. Purans, "Electronic structure of cubic ScF₃ from first-principles calculations," *Low Temp. Phys.* **42**, 556 (2016); H. B. Hamed, A. Qteish, N. Meskini, and M. Alouani, "Calculated hybrid and semilocal functionals and *GW* electronic structure of the metal trifluorides MF₃ (*M* = Sc, Y, Al)," *Phys. Rev. B* **92**, 165202 (2015).
- ¹⁹ S. U. Handunkanda, E. B. Curry, V. Voronov, A. H. Said, G. G. Guzmán-Verri, R. T. Brierley, P. B. Littlewood, and J. N. Hancock, "Large isotropic negative thermal expansion above a structural quantum phase transition," *Phys. Rev. B* **92**, 134101 (2015).
- ²⁰ A. van Roekeghem, J. Carrete, and N. Mingo, "Anomalous thermal conductivity and suppression of negative thermal expansion in ScF₃," *Phys. Rev. B* **94**, 020303 (2016).
- ²¹ B. K. Greve, K. L. Martin, P. L. Lee, P. J. Chupas, K. W. Chapman, and A. P. Wilkinson, "Pronounced negative thermal expansion from a simple structure: cubic ScF₃," *J. Am. Chem. Soc.* **132**, 15496 (2010).
- ²² Chen W. Li, Xiaoli Tang, J. A. Muñoz, J. B. Keith, S. J. Tracy, D. L. Abernathy, and B. Fultz, "Structural relationship between negative thermal expansion and quartic anharmonicity of cubic ScF₃," *Phys. Rev. Lett.* **107**, 195504 (2011).
- ²³ K. S. Aleksandrov, V. N. Voronov, A. N. Vtyurin, A. S. Krylov, M. S. Molokeev, M. S. Pavlovskii, S. V. Goryainov, A. Yu. Likhacheva, and A. I. Ancharov, "Pressure-induced phase transition in the cubic ScF₃ crystal," *Phys. Solid State* **51**, 810 (2009).
- ²⁴ K. S. Aleksandrov, V. N. Voronov, A. N. Vtyurin, S. V. Goryainov, N. G. Zamkova, Zinenko V. I., and A. S. Krylov, "Lattice dynamics and hydrostatic-pressure-induced phase transitions in ScF₃," *JETP* **94**, 997 (2002).
- ²⁵ R. A. Cowley, "Structural phase transitions I. Landau theory," *Adv. Phys.* **29**, 1 (1980).
- ²⁶ J. C. Slonczewski and H. Thomas, "Interaction of elastic strain with the structural transition of strontium titanate," *Phys. Rev. B* **1**, 3599 (1970).
- ²⁷ Ll. Mañosa and A. Planes, "Materials with giant mechanocaloric effects: cooling by strength," *Adv. Mat.* **29**, 1603607 (2017); B. Lu and J. Liu, "Mechanocaloric materials for solid-state cooling," *Sci. Bull.* **60**, 1638 (2015); X. Moya, S. Kar-Narayan, and N. D. Mathur, "Caloric effects near ferroic transitions," *Nat. Mater.* **13**, 439 (2014).
- ²⁸ Ll. Mañosa, D. González-Alonso, A. Planes, E. Bonnot, M. Barrio, J.-Ll. Tamarit, S. Aksoy, and M. Acet, "Giant solid-state barocaloric effect in the Ni-Mn-In magnetic shape-memory alloy," *Nat. Mater.* **9**, 478 (2010).
- ²⁹ Ll. Mañosa, D. González-Alonso, A. Planes, M. Barrio, J.-Ll. Tamarit, I. S. Titov, M. Acet, A. Bhattacharyya, and S. Majumdar, "Inverse barocaloric effect in the giant magnetocaloric La-Fe-Si-Co compound," *Nat. Commun.* **2**, 595 (2011).
- ³⁰ I. N. Flerov, M. V. Gorev, A. Tressaud, and N. M. Laptash, "Perovskite-like fluorides and oxyfluorides: phase transitions and caloric effects," *Crystallogr. Rep.* **56**, 9 (2011).
- ³¹ Y. Suheyli, M. Barrio, B. Emre, E. Stern-Taulats, A. Planes, J.-Ll. Tamarit, Y. Mudryk, K. A. Gschneidner Jr., and Ll. Pecharsky, V. K. and? Mañosa, "Barocaloric effect in the magnetocaloric prototype Gd₅Si₂Ge₂," *Appl. Phys. Lett.* **101**, 071906 (2012).
- ³² E. Stern-Taulats, A. Planes, P. Lloveras, M. Barrio, J.-Ll. Tamarit, S. Pramanick, S. Majumdar, C. Frontera, and Ll. Mañosa, "Barocaloric and magnetocaloric effects in Fe₄₉Rh₅₁," *Phys. Rev. B* **89**, 214105 (2014).
- ³³ D. Matsunami, A. Fujita, K. Takenaka, and M. Kano, "Giant barocaloric effect enhanced by the frustration of the antiferromagnetic phase in Mn₃GaN," *Nat. Mater.* **14**, 73 (2015).
- ³⁴ P. Lloveras, E. Stern-Taulats, M. Barrio, J. Tamarit, S. Crossley, W. Li, V. Pomjakushin, A. Planes, Ll. Mañosa, N. D. Mathur, and X. Moya, "Giant barocaloric effect at low pressure in ferroelectric ammonium sulphate," *Nat. Commun.* **6**, 1 (2015).
- ³⁵ E. Stern-Taulats, P. Lloveras, M. Barrio, E. Defay, M. Egilmez, A. Planes, J.-Ll. Tamarit, Ll. Mañosa, N. D. Mathur, and X. Moya, "Inverse barocaloric effects in ferroelectric BaTiO₃ ceramics," *APL Mater.* **4**, 091102 (2016).
- ³⁶ J. M. Bermúdez-García, M. Sánchez-Andújar, and S. Castro-García, "Giant barocaloric effect in the ferroic organic-inorganic [TPrA][Mn(dca)₃] perovskite under easily accessible pressures hybrid," *Nat. Commun.* **8**, 15715 (2017).
- ³⁷ Piskunov, S. and Žgurs, P. A. and Bocharov, D. and Kuzmin, A. and Purans, J. and Kalinko, A. and Evarestov, R. A. and Ali, S. E. and Rocca, F., "Interpretation of unexpected behavior of infrared absorption spectra of scf₃ beyond the quasiharmonic approximation," *Phys. Rev. B* **93**, 214101 (2016).
- ³⁸ Y. Liu, Z. Wang, M. Wu, Q. Sun, M. Chao, and Y. Jia, "Negative thermal expansion in isostructural cubic ReO₃ and ScF₃: a comparative study," *Comput. Mat. Sc.* **107**, 157 (2015).
- ³⁹ V. I. Zinenko and N. G. Zamkova, "Lattice dynamics of MF₃ crystals (*M* = Al, Ga, and In)," *Phys. Solid State* **42**, 1348–1353 (2000).
- ⁴⁰ B. A. Strukov and A. P. Levanyuk, *Ferroelectric Phenomena in Crystals: Physical Foundations* (Springer, 1964).
- ⁴¹ P. J. Chupas, S. Chaudhuri, J. C. Hanson, X. Qiu, P. L. Lee, S. D. Shastri, S. J. L. Billinge, and C. P. Grey, "Probing local and long-range structure simultaneously: an in situ study of the high-temperature phase transition of α -AlF₃," *J. Am. Chem. Soc.* **126**, 4756 (2004).
- ⁴² M. G. Stachiotti, F. Corà, C. R. A. Catlow, and C. O. Rodriguez, "First-principles investigation of ReO₃ and related oxides," *Phys. Rev. B* **55**, 7508 (1997).
- ⁴³ T. Chatterji, P. G. Freeman, M. Jimenez-Ruiz, R. Mittal, and S. L. Chaplot, "Pressure- and temperature-induced *M*₃ phonon softening in ReO₃," *Phys. Rev. B* **79**, 184302 (2009).
- ⁴⁴ Tapan Chatterji and G.J. McIntyre, "Pressure-induced structural phase transition in ReO₃," *Solid State Commun.* **139**, 12 (2006).
- ⁴⁵ A recent first-principles calculation⁵⁷ has suggested that the c-c transition is weakly first-order.
- ⁴⁶ E. Suzuki, Y. Kobayashi, S. Endo, and T. Kikegawa,

- “Structural phase transition in ReO_3 under high pressure,” *J. Phys: Cond. Matt.* **14**, 10589 (2002); J.-E. Jørgensen, J. Staun Olsen, and L. Gerward, “Phase transitions in ReO_3 studied by high-pressure X-ray diffraction,” *J. Appl. Crystallogr.* **33**, 279 (2000).
- ⁴⁷ E. E. Rodriguez, A. Llobet, T. Proffen, B. C. Melot, R. Seshadri, P. B. Littlewood, and A. C. Cheetham, “The role of static disorder in negative thermal expansion in ReO_3 ,” *J. Appl. Phys.* **105**, 114901 (2009).
- ⁴⁸ T. Chatterji, T. C. Hansen, M. Brunelli, and P. F. Henry, “Negative thermal expansion of ReO_3 in the extended temperature range,” *Appl. Phys. Lett.* **94**, 241902 (2009).
- ⁴⁹ T. Chatterji, P. F. Henry, R. Mittal, and S. L. Chaplot, “Negative thermal expansion of ReO_3 : neutron diffraction experiments and dynamical lattice calculations,” *Phys. Rev. B* **78**, 134105 (2008).
- ⁵⁰ F. Corà, M. G. Stachiotti, C. R. A. Catlow, and C. O. Rodriguez, “Transition metal oxide chemistry: electronic structure study of WO_3 , ReO_3 , and NaWO_3 ,” *The Journal of Phys. Chem. B* **101**, 3945 (1997).
- ⁵¹ H. Hamdi, E. K. H. Salje, P. Ghosez, and E. Bousquet, “First-principles reinvestigation of bulk WO_3 ,” *Phys. Rev. B* **94**, 245124 (2016).
- ⁵² F. Corà, A. Patel, N. M. Harrison, R. Dovesi, and C. R. A. Catlow, “An ab initio hartree-fock study of the cubic and tetragonal phases of bulk tungsten trioxide,” *J. Am. Chem. Soc.* **118**, 12174–12182 (1996).
- ⁵³ W. L. Kehl, R. G. Hay, and D. Wahl, “The structure of tetragonal tungsten trioxide,” *J. of App. Phys.* **23**, 212 (1952).
- ⁵⁴ M. Sato, B. H. Grier, G. Shirane, and T. Akahane, “Successive structural phase transitions in Na_xWO_3 ,” *Phys. Rev. B* **25**, 6876 (1982).
- ⁵⁵ H. Sowa and H. Ahsbabs, “Pressure-induced octahedron strain in VF_3 -type compounds,” *Acta Crystallogr. Sec. B* **54**, 578 (1998).
- ⁵⁶ J.-E. Jørgensen, W. G. Marshall, and R. I. Smith, “The compression mechanism of CrF_3 ,” *Acta Crystallogr. Sec. B* **60**, 669 (2004).
- ⁵⁷ D. V. S. Muthu, P. Teredesai, S. Saha, Suchitra, U. V. Waghmare, A. K. Sood, and C. N. R. Rao, “Pressure-induced structural phase transitions and phonon anomalies in ReO_3 : Raman and first-principles study,” *Phys. Rev. B* **91**, 224308 (2015).